XUV interferometry using high-order harmonics: Application to plasma diagnostics

Hergott, JF; Salieres, P; Merdji, H; Le Deroff, L; Carre, B; Auguste, T; Monot, P; D'Oliveira, P; Descamps, D; Norin, Johan; Lyngå, C; L'Huillier, Anne; Wahlström, Claes-Göran; Bellini, M; Huller, S

Published in:
Laser and Particle Beams

DOI:
10.1017/S0263034601191056

2001

Laser and Particle Beams (2001), *19*, 35–40. Printed in the USA.

XUV interferometry using high-order harmonics: Application to plasma diagnostics

J.-F. HERGOTT,[1] P. SALIÈRES,[1] H. MERDJI,[1] L. LE DÉROFF,[1] B. CARRÉ,[1] T. AUGUSTE,[1] P. MONOT,[1] P. D'OLIVEIRA,[1] D. DESCAMPS,[2] J. NORIN,[2] C. LYNGÅ,[2] A. L'HUILLIER,[2] C.-G. WAHLSTRÖM,[2] M. BELLINI,[3] AND S. HULLER[4]

[1]Service des Photons, Atomes et Molécules, CEA-DSM-DRECAM, Centre de Saclay, 91191 Gif-sur-Yvette, France
[2]Department of Physics, Lund Institute of Technology, P.O. Box 118, S-221 00 Lund, Sweden
[3]L.E.N.S., Largo E. Fermi, 2, I-50125 Florence, Italy
[4]Centre de Physique Théorique, CNRS, Ecole Polytechnique, 91128 Palaiseau, France

(RECEIVED 1 December 2000; ACCEPTED 5 February 2001)

Abstract

In this paper, we present and compare the two different XUV interferometric techniques using high-order harmonics that have been developed so far. The first scheme is based on the interference between two spatially separated phase-locked harmonic sources while the second uses two temporally separated harmonic sources. These techniques have been applied to plasma diagnostics in feasibility experiments where electron densities up to a few 10^{20} e^-/cm^3 have been measured with a temporal resolution of 200 fs. We present the main characteristics of each technique and discuss their respective potentials and limitations.

1. INTRODUCTION

High-order harmonic generation (HHG) in gases is now a widely studied nonlinear process. The research in this domain shows two main directions. On the one hand, researchers are working on the different fundamental aspects involved in high-order generation. On the other hand, they have developed several applications of this unique XUV source. High-order harmonics present a good beam quality, which allows focusing the harmonic radiation to very tight spots (Le Déroff *et al.*, 1998; Schnürer *et al.*, 2000), a high brightness and a high repetition rate (up to 1 kHz) (Constant *et al.*, 1999; Schnürer *et al.*, 1999; Hergott *et al.*, in prep.). Since HHG is a field-driven process, the properties of the laser that is used to generate the harmonics are partially transferred to the XUV radiation. As a result, the harmonic pulse presents a short duration, equal to or shorter than the generating laser pulse duration (Bouhal *et al.*, 1998; Kobayashi *et al.*, 1998) depending on the harmonic order. The harmonic radiation is also naturally synchronized with the fundamental driving IR laser. These last two properties are very important for experiments of the pump probe type. Up to now, high-order harmonics have been used in atomic and molecular spectroscopy (Larsson *et al.*, 1995; Gisselbrecht *et al.*, 1999). This type of experiment can also be applied in solid-state physics, for instance, to probe the relaxation of electrons excited in the conduction band of a dielectric material (Quéré *et al.*, 2000). Another important property of the harmonic source is the good temporal (Bellini *et al.*, 1998) and spatial (Salières *et al.*, 1995; Ditmire *et al.*, 1996; Le Déroff *et al.*, 2000) coherence that can be obtained in some generation conditions. Finally, a very unique property in this XUV range is the possibility of producing two mutually coherent sources either separated in space or in time, opening the way to original interferometric schemes. Due to its short wavelength and short pulse duration, the harmonic radiation is well suited to time-resolved plasma diagnostics (Theobald *et al.*, 1996). Indeed, the plasma refraction index is $n^2 = 1 - n_e/n_{cr}$ where n_e is the electronic density and n_{cr} the critical density. When $n_e > n_{cr}$, the probe beam cannot penetrate in the plasma and is reflected. For IR light at 800 nm $n_{cr} = 1.7 \cdot 10^{21}$ e^-/cm^3 whereas for XUV light at 72 nm $n_{cr} = 2 \cdot 10^{23}$ e^-/cm^3. Therefore harmonics are able to penetrate high density plasmas and are less sensitive to the beam refraction induced by sharp density gradients. In the two first sections, we present the spatial and spectral interferometry schemes and the last section is dedicated to a comparison of the two schemes.

Address correspondence and reprint requests to: J.-F. Hergott, Service des Photons, Atomes et Molécules, Bât. 524, CEA-DSM-DRECAM, Centre de Saclay, 91191 Gif-sur-Yvette, France. E-mail: hergott@drecam.cea.fr.

2. SPATIAL INTERFEROMETRY AND APPLICATION TO DENSE PLASMA DIAGNOSTICS

Zerne *et al.* (1997) have demonstrated the possibility of producing two phase-locked harmonic sources, separated *in space* by splitting the generating fundamental laser beam into two parts focused at two different places in a gas jet. The two harmonic beams that are produced interfere coherently when they overlap in the far field after propagation. Indeed when splitting the laser beam into two spatially separated beams, we in fact perform a Young experiment at the laser frequency. Since HHG is a field-drive process, the phase locking is transferred to the generated harmonic beams giving rise to fringes in the harmonic far-field pattern. The IR laser pulse is split into two identical pulses with a setup resembling a Michelson interferometer set at zero time delay. Note that when varying this delay, one can study the temporal coherence of the harmonic emission (Bellini *et al.*, 1998; Lyngå *et al.*, 1999). One of the arms is slightly tilted so that the laser beams are focused in the gas jet at two spatially separated foci, where two harmonic sources are generated. A monochromator is used to select a given harmonic order. The far-field fringe pattern can be recorded either with a XUV charge coupled device (CCD) camera or with microchannel plates (MCP) coupled to a phosphor screen and a CCD. This setup was used in Saclay, at LUCA laser facility to study the produced interferences. The monochromator was composed of a toroidal mirror and a flat grating. The fringe pattern resulting from the far field interference exhibits a fringe period $\Delta i = \lambda d/a$ where λ is the wavelength of the harmonic, d the observation distance (set here to 0.5 m), and a the separation between the two phase-locked sources. In Figure 1a, one can see the linear variation of the fringe period as a function of the harmonic wavelength for two harmonic sources separated by a fixed distance $a = 100$ μm. The measured fringe contrast, in our generating conditions, was as high as 90% over a large spectral range (60 nm–40 nm) and decreased to 50% for shorter wavelengths. This decrease of the contrast is mainly due to the limitation imposed by the MCP resolution estimated to 80 μm (Le Déroff *et al.*, 2000). Note that in order to increase the effective spatial resolution, we have tilted the MCP to a grazing incidence of 12° that explains that the cross section of the beam is larger in the vertical dimension. We also observed the inverse linear variation of the fringe period as a function of the separation distance a between the two harmonic sources for the 17th harmonic as shown in Figure 1b. One can observe a good fringe contrast, over 90% for a 180-μm separation between the sources. This contrast stays over 30% even when the two sources are widely separated from each other ($a = 600$ μm). This gives evidence of a good mutual coherence of the two harmonic sources, even for a large spacing, which can be very useful for applications.

The *spatial* interferometry should be a powerful tool for probing dephasing objects. Indeed since the two harmonic beams are clearly separated by some 100 μm, one can put a dephasing object in one of the arms without perturbing the other one. The aim of the experiment we performed at the Lund Laser Center was to demonstrate that this technique can be used to probe a laser-produced plasma (Descamps *et al.*, 2000; Merdji *et al.*, 2000). In the following, we recall the main results. Figure 2a shows the experimental setup. Using the tunability of the HHG, we were able to choose a wavelength for the probe that minimizes refraction (by the density gradient), reflection, or absorption due to the plasma. The plasma probed was generated by focusing a 50-mJ 300-ps IR laser on a 50-μm thick Al foil fixed on a flat glass plate placed a few centimeters after the gas jet (see Fig. 2a). The plasma expands in the normal direction and perturbs the harmonic beam that is closer to the target. The delay between the harmonic pulses and the pump pulse is held constant to 1.2 ns. In Figure 2b is shown the fringe pattern without plasma. When the plasma is generated, there appears a clear distortion with a tilt of the fringes (Fig. 2c). To estimate the electron density of the plasma, we can approximate the observed fringe shift Φ at wavelength λ as $\Phi = dn_e/2\lambda n_{cr}$ where d is the distance traveled by the probe beam in the plasma. This distance is experimentally estimated to be 0.1 mm. In Figure 2c are plotted the isodensity

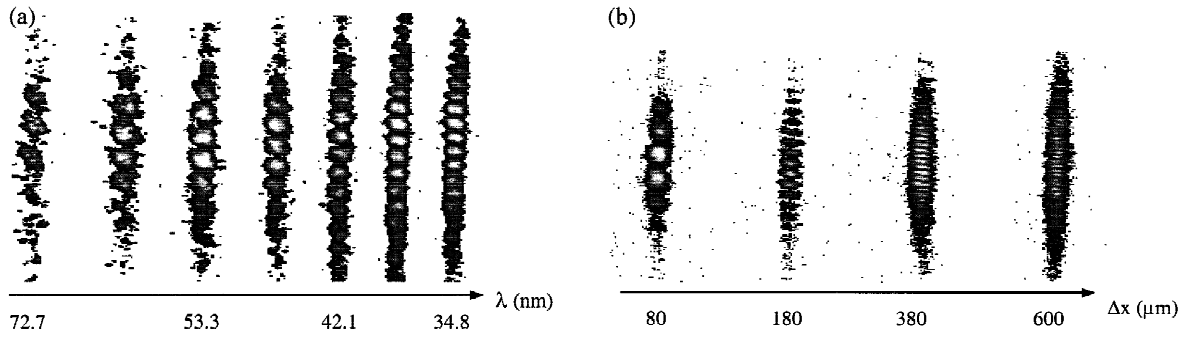

Fig. 1. Fringe pattern variation: (a) as a function of the harmonic wavelength for a 100-μm separation between the sources and (b) of the 17th harmonic as a function of the separation between the sources.

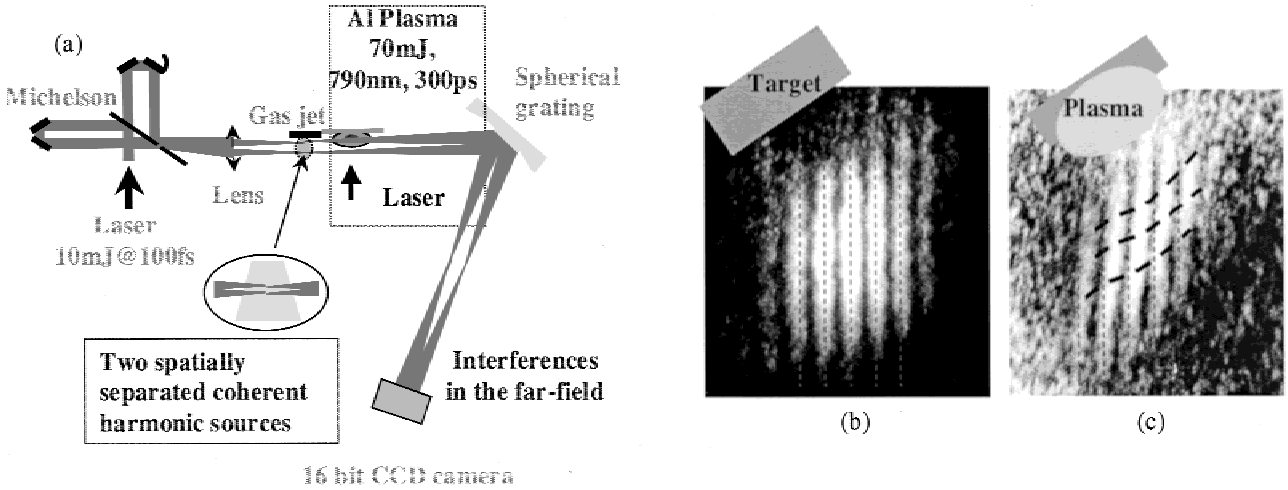

Fig. 2. (a) Experimental setup to produce two phase-locked harmonic sources and application experiments. Interference pattern with the 13th harmonic through an Al step filter. Single-shot fringe patterns of the 11th harmonic (b) without plasma, (c) with plasma. Initial fringe position (short dashed line) and isodensity lines (dashed curves).

curves corresponding, from bottom to top, to n_e of $0.5\cdot10^{20}$, $1\cdot10^{20}$, and $2\cdot10^{20}$ e^-/cm^3, assuming that the bottom part of the fringes is not perturbed. In Figure 3 is shown a simulation of the plasma expansion performed with a hydrodynamical code called MULTI (Ramis *et al.*, 1988) in the conditions of the experiment for different time delays. The electronic density falls down from the solid density to about 10^{21} after just a few microns expansion, whatever the expansion time. After a 1.2-ns expansion of the plasma, corresponding to the experimental pump-probe delay, the electron density decreases almost linearly from about $2\cdot10^{20}$ e^-/cm^3 close to the target surface ($\sim$20 μm) to a few 10^{19} e^-/cm^3 at 40 μm from the target surface. The shape of this density gradient is observed on the fringe pattern in Figure 2c. Indeed, the linear decrease of the density results in a global tilt of the fringes. We thus reproduce both the absolute value of the electron density and the density gradient.

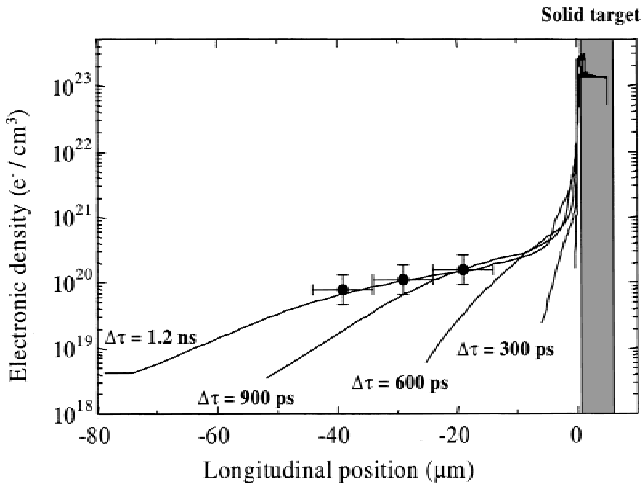

Fig. 3. Simulation with a hydrodynamical code of the plasma expansion in the experimental conditions (solid lines) and experimental points (full circles and error bars).

3. SPECTRAL INTERFEROMETRY AND APPLICATION TO TIME-RESOLVED PLASMA DIAGNOSTICS

Similar to the generation of two phase-locked harmonic sources separated in space, we have demonstrated that it is also possible to produce two phase-locked harmonic sources separated *in time* by focusing a double laser pulse in the generating medium (Salières *et al.*, 1999). After dispersion by a grating, the two harmonic pulses can overlap and interfere in the spectral domain giving rise to a highly contrasted spectral fringe pattern. This frequency domain interferometry is the temporal analog of Young's slits experiment. The double laser pulse was created by using the group velocity difference on the two axes of a birefringent plate rotated at 45° from the laser polarization. A polarizer placed after the plate projects both components on the same axis. The calibrated thickness of the plates fixed the time delay between the pulses (120 fs and 450 fs). This setup offers high stability, making possible acquisition over thousands of shots. The fringe period in the wavelength domain is now given by $\Delta\lambda = \lambda^2/c\Delta t$, where λ is the harmonic wavelength, c the light velocity and Δt the time delay between the two pulses. A high resolution spectrometer is necessary to perform the measurements. The experimental spectra of harmonics 11, 15, and 19 generated by two phase-locked laser pulses delayed by 120 fs and focused at $2\cdot10^{14}$ W/cm^2 in argon are shown in Figures 4a, 4b, and 4c, respectively. Regular contrasted fringes are measured for all orders, with a reduced contrast when the order increases: from 90% for harmonic 11 to about 45% for the 19th. The period of the fringes varies

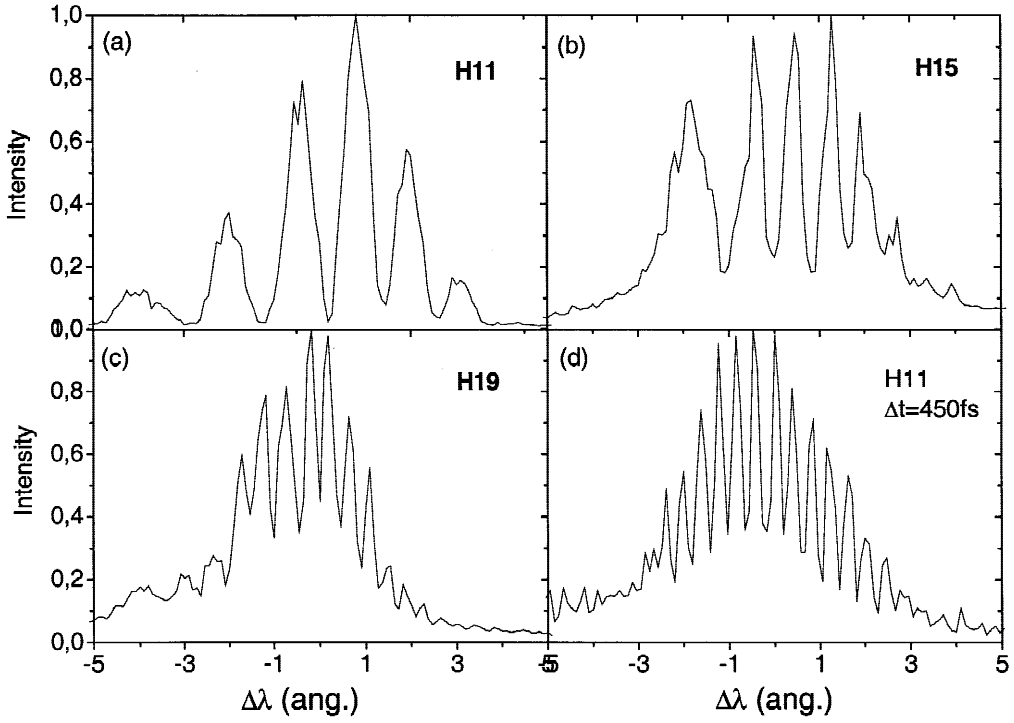

Fig. 4. Experimental spectra of harmonics 11 (a), 15 (b), and 19 (c) generated by two laser pulses delayed by 120 fs and focused at $2 \cdot 10^{14}$ W/cm^2. Experimental spectra of harmonic 11 (d) obtained at $3 \cdot 10^{14}$ W/cm^2 with a delay of 450 fs.

quadratically with the wavelength, as expected from the above formula. In Figure 4d is shown the experimental spectra for the 11th harmonic with a 450-fs time delay between the two phase-locked sources. The fringe period decreases as expected from the formula by more than a factor of 3 compared to Figure 4a. The contrast is reduced due to the higher laser intensity, which induces ionization of the medium.

Besides its fundamental interest, the above study opens up new perspectives for plasma diagnostics using XUV frequency-domain interferometry. As a demonstration, we probed the temporal evolution of the electron density in a He high density gas jet, ionized by an intense ultrashort laser pulse (50 fs, 10^{18} W/cm^2). The experimental setup shown in Figure 5a was installed at the Saclay UHI10 laser facility (Ti:Sapphire 800 mJ, 50 fs, 10 Hz). The two 11th harmonic pulses were generated in a xenon gas jet with a fixed 300-fs delay and refocused without magnification with a toroidal mirror into a helium jet. After analysis by an XUV flat-field spectrometer, the fringes were detected by MCP coupled to a phosphor screen and a CCD camera. To achieve the best spectral resolution, the MCP were tilted to a grazing incidence of 8°. The harmonic fringe pattern was recorded as a function of the delay τ between the TW pulse generating the plasma and the harmonic probe (zero delay for pump in between the two probes). In Figure 5b is shown the spatially integrated fringe pattern from single-shot images as a function of the pump-probe delay τ. A clear shift can be seen in the middle of the image, when the plasma is created in between the two harmonic pulses. The average shift is plotted in Figure 5c. The dashed curve is the theoretical shift obtained for the relevant experimental parameters. The calculated curve fits well the experimental one for an electron density of $6 \cdot 10^{19}$ cm^{-3}, which is in quite good agreement with the expected density ($4.8 \cdot 10^{19}$ cm^{-3}) assuming fully stripped ions. The slower shift of the fringes compared to the expected very fast optical field ionization front is, in fact, due to the geometry (probe at 45°) that lowers the time resolution to about 200 fs.

4. COMPARISON BETWEEN THE SPATIAL AND SPECTRAL INTERFEROMETRY TECHNIQUES

The two interferometry techniques present some common features. First of all, they are both performed without specific XUV optics (except for XUV monochromators). Indeed, the space or time splitting is realized on the IR laser beam, where it is easy to do so, and is naturally transferred on the two phase-locked harmonic sources. Imperfect and expensive XUV optics, such as XUV beam splitters, are thus avoided. The high brightness of the harmonic radiation allows the acquisition of single-shot fringe patterns, avoiding instability problems. The femtosecond temporal resolution, given by the harmonic pulse duration (typically a few tens of femtoseconds in our case) is another common feature of these techniques. The spectral interferometry experiment presented in Section 3 had a lower temporal resolution be-

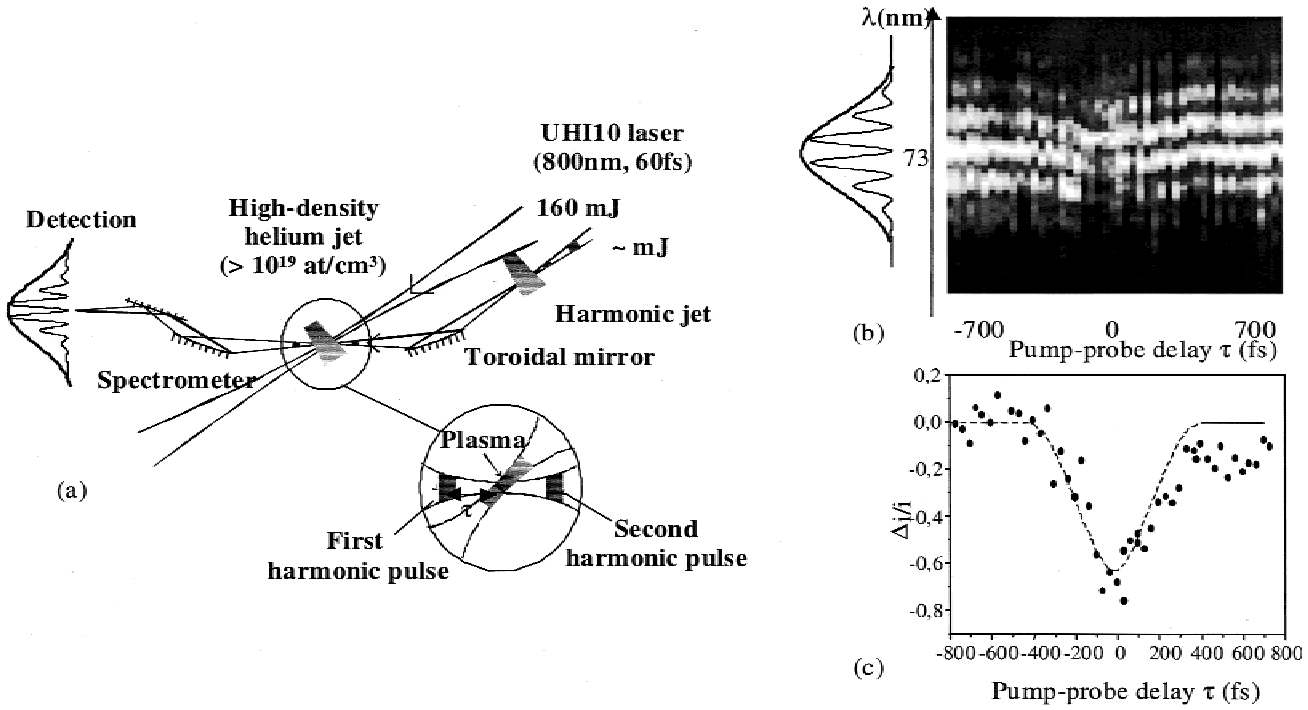

Fig. 5. (a) Experimental setup for the spectral interferometry with harmonics. Variation of the (b) spatially integrated fringe pattern and (c) average fringe shift with the delay between the plasma generating laser beam and the 11th harmonic beams.

cause of the 45° geometry of the setup that results in a mixing of the temporal and spatial dimensions. However, a collinear geometry, where pump and probes propagate along the same axis, would ensure a resolution given by the harmonic pulse duration.

A first difference between the two techniques is that the observed fringe period varies linearly with the wavelength in the spatial case, but quadratically in the spectral case. With the former, higher harmonic orders can thus be used for the measurements for a given detector resolution. Another difference is the necessity to preserve the reference beam in the spatial interferometry scheme. Indeed, the two harmonic beams have to be separated enough so that the expansion of the plasma in time will not affect the reference beam. Otherwise, the absolute reference is lost. This technique is thus better suited to the study of small dephasing objects (a few hundred microns). In the case of spectral interferometry, the *same* medium (spatially) is probed by the two harmonic beams but with a time delay Δt, so that this technique is sensitive only to the medium temporal evolution. Note that arbitrary large delays τ relative to the pump beam can be probed regardless of the delay Δt between the harmonic beams: we simply evolve from an absolute measurement (when the plasma is generated in between the two probes) to a relative one (when it is generated before). Scanning all the delays allows us, thanks to the initial absolute reference, to map precisely the whole (absolute) evolution of the system. Another important difference is that the spatial interferometry gives a 2D map of the plasma. Note however that in the scheme presented in Section 2, there is no true imaging of the plasma, simply a projection in the far field, which means that the spatial resolution is degraded due to diffraction. In the spectral interferometry, the plasma was imaged in the spectral plane of the monochromator, giving a 1D image (even though there was no magnification of this spatial dimension). The other dimension is taken by the spectral dispersion. Since in principle all the fringes are shifted by the same amount, a very high precision on the phase shift can be obtained thanks to this redundant information. Combining a magnification system to the spectral system would give a good temporal and spatial resolution (in one dimension) of the plasma diagnostic (note that imaging implies the use of a slit perpendicular to the dispersion direction so as not to mix up all the dephasings present in this spatial dimension). Such more sophisticated systems are under study to go further in the applications of these interferometric techniques to plasma diagnostics.

In conclusion we have studied the possibility of performing interferometry in the XUV range with high-order harmonics in the *spatial* as well as in the *frequency* domain. This is made possible by using the mutual coherence (in space or in time) of two separated harmonic sources. These results are not only interesting from a fundamental point of view, they also open the possibility of new applications of the harmonic light in time-resolved interferometric experiments, for example, measurements of high electron densities in ultrashort transient plasmas with a femtosecond resolution. These two interferometric techniques are com-

plementary and present different limitations that will be partially or totally overcome in the future designs. The work carried out in Lund (plasma diagnostic with the spatial interferometry technique) was supported by the European Community under contract No. ERBFMGECT950020 and No. ERBFMBICT983348, by the Swedish Natural Science Research Council and by the Göran Gustafsson's Foundation for Medicine and Natural Science.

REFERENCES

Bellini, M., Lyngå, C., Tozzi, A., Gaarde, M.B., Hänsch, T.W., L'Huillier, A. & Wahlström, C.G. (1998). *Phys. Rev. Lett.* **81**, 297.

Bouhal, A., Salières, P., Breger, P., Agostini, P., Hamoniaux, G., Mysirowicz, A., Antonetti, A., Constantinescu, R. & Muller, H.G. (1998). *Phys. Rev. A* **58**, 389.

Constant, E., Garzella, D., Breger, P., Mével, E., Dorrer, C., Le Blanc, C., Salin, F. & Agostini, P. (1999). *Phys. Rev. Lett.* **82**, 1668.

Descamps, D., Hergott, J.F., Merdji, H., Salières, P., Lyngå, C., Norin, J., Bellini, M., Hänsch, T.W., L'Huillier, A. & Wahlström, C.G. (2000). *Opt. Lett.* **25**, 135.

Ditmire, T., Grumbell, E.T., Smith, R.A., Tisch, J.W.G., Meyerhofer, D.D. & Hutchinson, M.H.R. (1996). *Phys. Rev. Lett.* **77**, 4756.

Gisselbrecht, M., Descamps, D., Lynga, C., L'Huillier, A., Wahlström, C.G. & Meyer, M. (1999). *Phys. Rev. Lett.* **82**, 4607.

Kobayashi, Y., Sekikawa, T., Nabekawa, Y. & Watanabe, S. (1998). *Opt. Lett.* **23**, 64.

Larsson, J., Mével, E., Zerne, R., L'Huillier, A., Wahlström, C.G. & Svanberg, S. (1995). *J. Phys. B* **L53**, 28.

Le Déroff, L. Salières, P. & Carré, B. (1998) *Opt. Lett.* **23**, 1544.

Le Déroff, L., Salières, P. & Carré, B. (2000). *Phys. Rev. A* **61**, 043802.

Lyngå, C., Gaarde, M.B., Delfin, C., Bellini, M., Hänsch, T.W., L'Huillier, A. & Wahlström, C.G. (1999). *Phys. Rev. A* **60**, 4823.

Merdji, H., Salières, P., Le Déroff, L., Hergott, J.F., Carré, B., Joyeux, D., Descamps, D., Lyngå, C., Norin, J., L'Huillier, A., Wahlström, C.G., Bellini, B.M. & Huller, S. (2000). *Laser Part. Beams* **18**, 495.

Quéré, F., Guizard, S., Martin, P., Petite, G., Merdji, H., Carré, B., Hergott, J.F. & Le Déroff, L. (2000). *Phys. Rev. B.* **15**, 61.

Ramis, R., Schmalz, R. & Meyer-Ter-Vehn, J. (1988). *Comput. Phys. Commun.* **49**, 475.

Salières, P., L'Huillier, A. & Lewenstein, M. (1995). *Phys. Rev. Lett.* **74**, 3776.

Salières, P., Le Déroff, L., Auguste, T., Monot, P., d'Oliveira, P., Campo, D., Hergott, J.F., Merdji, H. & Carré, B. (1999). *Phys. Rev. Lett.* **83**, 5483.

Schnürer, M., Cheng, Z., Hentschel, M., Tempea, G., Kalman, P., Brabec, T. & Krausz, F. (1999). *Phys. Rev. Lett.* **83**, 722.

Schnürer, M., Cheng, Z., Hentschel, M., Krausz, F., Wilhein, T., Hambach, D., Schmahl, G., Drescher, M., Lim, Y. & Heinzmann, U. (2000). *Appl. Phys. B* **70** (Suppl.), 227.

Theobald, W., Hässner, R., Wülker, C. & Sauerbrey, R. (1996). *Phys. Rev. Lett.* **77**, 298.

Zerne, R., Altucci, C., Bellini, M., Gaarde, M.B., Hänsch, T.W., L'Huillier, A., Lyngå, C. & Wahlström, C.G. (1997). *Phys. Rev. Lett.* **79**, 1006.